Original Full Length Article

Partial loss of Smad7 function impairs bone remodeling, osteogenesis and enhances osteoclastogenesis in mice ☆

Nan Li [a], Wayne Yuk-Wai Lee [b], Si-En Lin [b], Ming Ni [b], Ting Zhang [b], Xiao-Ru Huang [c], Hui-Yao Lan [c], Gang Li [a,b,d,e,*]

[a] Key Laboratory for Regenerative Medicine, Ministry of Education, School of Biomedical Sciences, Faculty of Medicine, The Chinese University of Hong Kong, Hong Kong, China
[b] Department of Orthopaedics & Traumatology, Faculty of Medicine, The Chinese University of Hong Kong, Hong Kong, China
[c] Department of Medicine & Therapeutics, Faculty of Medicine, The Chinese University of Hong Kong, Hong Kong, China
[d] Stem Cells and Regenerative Medicine Laboratory, Li Ka Shing Institute of Health Sciences, The Chinese University of Hong Kong, Prince of Wales Hospital, Hong Kong, China
[e] The CUHK-ACC Space Medicine Centre on Health Maintenance of Musculoskeletal System, The Chinese University of Hong Kong Shenzhen Research Institute, Shenzhen, China

ARTICLE INFO

ABSTRACT

Smad7 is well demonstrated as a negative regulator of TGF-β signaling. Its alteration in expression often results in diseases such as cancer and fibrosis. However, the exact role of Smad7 in regulating bone remodeling during mammalian development has not been properly delineated. In this study we performed experiments to clarify the involvement of Smad7 in regulating osteogenesis and osteoclastogenesis both in vivo and in vitro. Genetically engineered Smad7$^{\Delta E1}$ (KO) mice were used, whereby partial functional of Smad7 is lost by deleting exon I of the Smad7 gene and the truncated proteins cause a hypomorphic allele. Analysis with μCT imagery and bone histomorphometry showed that the KO mice had lower TbN, TbTh, higher TbSp in the metaphysic region of the femurs at 6, 12, 24 weeks from birth, as well as decreased MAR and increased osteoclast surface compared with the WT mice. In vitro BM-MSC multi-lineage differentiation evaluation showed that the KO group had reduced osteogenic potential, fewer mineralized nodules, lower ALP activity, and reduced gene expression of Col1A1, Runx2 and OCN. The adipogenic potential was elevated in the KO group with more formation of lipid droplets, and increased gene expression of Adipsin and C/EBPα. The osteoclastogenic potential of KO mice BMMs was elevate, with emergence of more osteoclasts, larger resorptive areas, and increased gene expression of TRAP and CTR. Our results indicate that partial loss of Smad7 function in mice leads to compromised bone formation and enhanced bone resorption. Thus, Smad7 is acknowledged as a novel key regulator between osteogenesis and osteoclastogenesis.

© 2014 Elsevier Inc. All rights reserved.

Introduction

Bone is a metabolically active and high energy consuming tissue, which is continuously remodeled, shaped and repaired through its lifetime. This intricate process is carried out by two key cells: osteoblasts and osteoclasts. Osteoblasts, bone matrix depositing cells derived from mesenchymal stem cells, give rise to osteocytes. Osteoclasts are specialized bone resorptive cells derived from hematopoietic progenitor cells embedded in bone marrow, which also give rise to macrophages in tissue and monocytes in peripheral blood [1]. The cellular coupling activities between osteoclasts and osteoblasts are tightly regulated by local and global systemic factors, which provide stable bone homeostasis or bone remodeling following tissue damage [2]. Disruption of this equilibrium often can give rise to various musculoskeletal disorders including osteoporosis, osteoporosis, osteopenia and arthritis.

TGF-β (transforming growth factor β) is a universal, multifactorial cytokine that is regulating proliferation, differentiation and apoptosis in a broad range of tissues during embryonic and postnatal life through trans-membrane receptors. Combinatorial interactions in the receptor and ligand complex allow differential signaling in the same tissues [3]. It is one of the most important factors in the bone environment, which simultaneously regulates the activities of both osteoblasts and osteoclasts, and hence the balance between the dynamic processes of bone formation and resorption. TGF-β family members signal through the canonical signaling pathway of SMAD (mothers against decapentaplegic and Sma related family) cascade [4]. There are three types of Smad proteins. The first is the receptor-regulated Smads (R-Smads), including

Smad2/3 for TGF-βs, and Smad1/5/8 for BMPs (bone morphogenetic proteins). They are directly phosphorylated by type I receptors, and form a complex with the second type of Smad proteins, Common Smad (Co-Smad, Smad4) prior to translocation into the nucleus where they regulate gene transcription [4,5]. The third type of Smad proteins, inhibitory Smads (I-Smads), including Smad6 and Smad7, are the key regulators for TGF-β signaling through negative-feedback mechanisms. Smad6 plays a more specific role in the BMP pathway, while Smad7 is a general antagonist for both TGF-β and BMP signaling [6–8].

Smad7 antagonizes TGF-β signaling pathway through multiple mechanisms inside both the cytoplasm and the nucleus [7,9]. It also serves as an important cross-talk mediator of the TGF-β signaling pathway with other signaling pathways [10]. Smad7 antagonizes TGF-β signaling in the cytoplasm by forming a stable complex with TGF-βRI and then inhibiting the recruitment and phosphorylation of R-Smads and R-Smad–Smad4 complex formation [11–13]. Furthermore, it is also an adaptor for recruitment of E3 ubiquitin ligases, like Smurf proteins for attachment on to the plasma membrane, thus inducing TGF-βRI endocytosis to mediate the ubiquitination and degradation of TGF-βRI in either the lysosomal or proteasomal pathways [14–17]. In addition, BMP and activin membrane-bound inhibitor (BAMBI) is able to form a ternary complex with activated TGF-βRI and Smad7, and synergizes with Smad7 to antagonize TGF-β signaling by interfering with the recruitment of R-Smads [18]. Inside the nucleus, Smad7 can interfere with the functional Smad–DNA complex formation as well [19,20]. Besides acting in the negative feedback loop in TGF-β signaling, Smad7 can also be transcriptionally induced by inflammatory cytokines through activation of NF-κB or STAT1, which in turn leads to suppression of TGF-β signaling [21,22].

Many studies have proved that altered expression of Smad7 often leads to human diseases, such as cancer, inflammatory diseases, diabetes and fibrosis [23–29]. While less is known of its role in the tissues of the skeletal system. It has been reported that loss of Smad3 signaling promotes callus formation via the concomitant upregulation of osteogenesis and suppression of chondrogenesis, which leads to faster fracture healing [30]. Smad7 has been reported to inhibit chondrocyte differentiation at multiple steps during endochondral ossification, and conditional overexpression of Smad7 in condensing mesenchymal cells shows reduced Sox9 expression and poor cartilage formation [31]. Other studies have also demonstrated that TGF-β acts directly on bone marrow macrophages (BMMs) and promotes osteoclastogenesis [32–34]. However, the specific role of Smad7 on bone remodeling has not been accurately delineated so far. So in this study, with Smad7$^{\Delta E1}$ (KO) mice in which partial functional of Smad7 is lost by deleting exon I of the Smad7 gene and the truncated proteins cause a hypomorphic Smad7 allele [35], we demonstrated the effect of partial loss of Smad7 on bone morphometry, lineage differentiation of bone marrow derived mesenchymal stem cells (BM-MSCs) and osteoclastogenesis of bone marrow macrophages (BMMs). The results of this study were designed to shed light on the precise role of Smad7 in bone remodeling and development.

Materials and methods

Study design

This study has been divided into three parts. In the first part, we studied long bone development using femurs from both WT and KO mice at 6, 12 and 24 weeks old. Left femurs were harvested and subjected to digital radiographs to compare the size and shape, to μCT examination to detect morphometric parameters as well as 3-D reconstruction images, and to bone histomorphometry assay to observe tissue morphology. In the second part, we compared the osteogenesis and adipogenesis potentials of BM-MSCs between the KO and WT mice. BM-MSCs were isolated from bone marrow and identified by flow cytometry. Histochemical staining and qRT-PCR were used to compare the differentiation potentials between the two groups. In the third part, bone marrow cells from both KO and WT mice were treated with M-CSF (recombinant murine macrophage-colony stimulating factor) and RANKL (receptor activator of nuclear factor kappa-B ligand) for osteoclastogenesis. TRAP staining, qRT-PCR, and bone resorption assay were used for comparison. Expression of phospho-Smad3 was observed in both osteogenesis and osteoclastogenesis processes.

Animals

Smad7$^{\Delta E1}$ mice (KO) were generated by inactivating the Smad7 gene in the mouse and replacing the translated part of exon I and part of intron I of the Smad7 genomic sequence, coding for the 204 N-terminal amino acid residues of Smad7, with a PGK-neo selection cassette as previously reported [35]. In these mice, the first half of the Smad7 protein is removed and the function of Smad7 is disrupted as partial loss [35]. All the animals were bred and supplied by LAN HY's Laboratory of The Chinese University of Hong Kong, and genotyped by PCR as described [36]. 5–6 week old KO and WT mice (CD-1 background mice, male, 20 g to 25 g) were used for the in vitro study. 6, 12, and 24 week old male mice were used for the in vivo study. All animal experiments were approved by the Animal Research Ethics Committee of The Chinese University of Hong Kong.

Isolation and culture of mice BM-MSCs

Mice were terminated by cervical dislocation. Both tibia and femurs were removed under sterile conditions. Bone marrow was flushed out and filtered through a 70-μm filter mesh to remove any bone spicules or cell clumps. The cells were then centrifuged at 300–400 g for 5 min and planted in 10-cm dishes at a density of 10^5 cells/cm². They were then incubated at 37 °C with 5% CO_2 in a humidified chamber. After 24 h, non-adherent cells were removed by changing medium. The medium was replaced with fresh one every three days till the cells were confluence. These cells were then passaged for further use.

Identification of mice BM-MSCs

The BM-MSCs were subjected to flow cytometry for cell surface expression of mice MSC positive markers CD90, CD44 and Sca1, as well as the negative markers CD34 and CD45. Briefly, cells at P4 were harvested and cell suspensions containing 1×10^5 cells were stained with the fluorescence conjugated antibodies: phycoerythrin (PE) conjugated rat anti-mouse CD44 IgG2b, PE conjugated rat anti-mouse CD90 and Sca-1 IgG2a, fluorescein isothiocyanate (FITC) conjugated rat anti-mouse CD45 and CD34 (all, BD Pharmingen, U.S.) for 1 h at 4 °C. After washing with PBS, the cells were re-suspended in 0.5 ml stain buffer (BD Pharmingen, U.S.). Non-specific background signals were measured by incubating the cells with the appropriate isotype control antibodies. The percentages of cells with positive signal were measured using a BD LSRFortessa Cell Analyzer, and data was analyzed using BD FACSDiva software.

Osteogenic differentiation assay

BM-MSCs of both KO and WT mice were plated at 4×10^3 cells/cm² in a 6-well plate and cultured in complete α-MEM medium (including 10% FBS) or osteogenic medium, for 7 and 14 days. The osteogenic medium was a complete medium supplemented with 1 nM dexamethasone, 50 μM ascorbic acid, and 10 mM β-glycerophosphate (all, Sigma-Aldrich, U.S.). Mineralized nodule formation was assessed using Alizarin Red S staining, the cell/matrix layer was washed with PBS, fixed with 70% ethanol, stained with 0.5% Alizarin Red S (pH 4.1, Sigma-Aldrich, U.S.) for 10 min, and viewed with a LEICA DMIRB microscope (Leica Cambridge Ltd., U.K.). To quantify the amount of Alizarin Red S bound to the mineralized nodules, the acetic acid extraction method was used, as reported

[37]. The mRNA expression of early and late osteogenic markers including *Collagen type1, alpha 1* (*Col1A1*), *Runt-related transcription factor 2* (*Runx2*) and *Osteocalcin* (*OCN*) was examined using qRT-PCR. The Alkaline Phosphatase (ALP) cytochemical staining was performed by an AP staining kit (Promega, U.S.). In brief, after fixation and equilibration with ALP buffer (0.15 M NaCl, 0.1 M Tris–HCl pH 9.0, 1 mM $MgCl_2$ and 0.1% Tween-20), the cells were incubated in ALP substrate solution (0.5 mg nitro-blue tetrazolium chloride (NBT) and 0.25 mg 5-bromo-4-chloro-3′-indolyphosphate p-toluidine salt (BCIP) in 1 ml ALP buffer) for 20 min at 37 °C. The color reaction was stopped by washing with distilled water and the positive stain appeared deep blue. The ALP activity was also performed by a LabAssay™ALP kit (Wako, U.S.). In brief, production of p-nitrophenol was measured at OD 405 nm for 15 min at 37 °C, based on the standard curve prepared with different concentrations of p-nitrophenol. The linear portion of the product curve was used for the calculation of enzyme activity by linear regression. The ALP activity was expressed as nmol p-nitrophenol per minute per μg protein.

Cell proliferation assay and colony forming assay

Cell proliferation was compared by using a BrdU assay kit (Roche Applied Science, U.S.). BM-MSCswere plated in triplicate at 5000 cells/well in 96-well plate and cultured either in complete α-MEM medium or osteogenic medium for 1, 3, and 6 days. After labelling with sterile BrdU labelling reagent at 37 °C for 3 h, the cells were then fixed with FixDenat solution and incubated with anti-BrdU antibodies (peroxidase conjugated for 1 h) for 90 min. The cells were then washed by PBS and incubated in substrate solution to perform a peroxidase reaction. The absorbance at 450 nm was measured and reported.

The colony-forming unit (CFU) assay was also performed. BM-MSCs plated in triplicate at 100 cells/well in 6-well plates and cultured either in complete α-MEM medium or osteogenic medium (3 days after α-MEM medium) for 10 days. The cells were fixed and stained with 1% crystal violet (Sigma-Aldrich, U.S.). Cell colonies were counted under microscopy and the CFU-F efficiency was performed according to the formula: CFU-F efficiency = (counted CFU-F / cells originally seeded) × 100. Triple CFU-F assays were performed for each isolated cell population.

Adipogenic differentiation assay

BM-MSCs from both groups were incubated in complete α-MEM medium (including 10% FBS) or adipogenic medium, for 7, 14 and 21 days for the assessment. The adipogenic medium was a complete medium supplemented with 500 nM dexamethasone, 50 μM indomethacin, 0.5 mM isobutylmethylxanthine, and 10 μg/ml insulin (all, Sigma-Aldrich, U.S.). Lipid droplet formation was assessed using Oil Red-O staining, the cell/matrix layer was washed with PBS three times, fixed with 70% ethanol, stained with 0.3% fresh Oil Red-O solution (Sigma-Aldrich, U.S.) for 30 min, and viewed with a LEICA DMIRB microscope (Leica Cambridge Ltd., U.K.). The mRNA expression of adipogenic markers including *CCAAT/enhancer binding protein alpha* (*C/EBPα*) and *Complement Factor D* (*Adipsin*) was examined using qRT-PCR.

Osteoclastogenesis assay

Bone marrow cells were isolated, filtered, centrifuged, re-suspended and cultured in complete α-MEM (including 10% FBS) supplemented with 10 ng/ml M-CSF until the bone marrow macrophages reached confluence. Cell dissociation reagent StemPro Accutase (Life Technologies, U.S.) was used for cell detachment and the cells were seeded at a density of 2.5×10^4/well in a 12-well plate and cultured with complete α-MEM supplemented with 10 ng/ml M-CSF (Life technologies, U.S.) and 100 ng/ml RANKL (supplied by Prof. Jia-ke XU's laboratory in The University of Western Australia), or M-CSF alone. After stimulation for

7 days, the cells were subjected to TRAP staining assay using an Acid Phosphatase, Leukocyte (TRAP) Kit (Sigma-Aldrich, U.S.). The mRNA expression of *Tartrate-resistant acid phosphatase* (*TRAP*) and *Calcitonin Receptor* (*CTR*) was examined using qRT-PCR. The bone resorption activity of the osteoclasts was assessed using HA/TCP coated plates (OAAS™, Oscotect INC., Korea). Areas of the bone resorption pitches on the plates were measured under a phase contrast microscope and quantified using Image-Pro Plus software (Version 6.0, U.S.).

Quantitative real-time-polymerase chain reaction (qRT-PCR)

Cells were harvested and lysed for RNA extraction with an RNeasy mini kit (Life Technologies, U.S.). The total RNA with the same nanograms was reverse-transcribed to cDNA by an M-MLV Reverse Transcriptase kit (Invitrogen™, U.S.). 3 μl of total cDNA of each sample was amplified in a final volume of 15 μl of reaction mixture containing Platinum SYBR Green qPCRSuperMix-UDG and specific primers for *C/EBPα*, *Adipsin*, *Col1A1*, *Runx2*, *OCN*, *Smad7*, *TRAP*, *CTR*, *18S* or *GAPDH* (all from TechDragon, HK; Table 1) using the ABI StepOnePlus™real-time PCR system. Cycling conditions were denaturation at 95 °C for 10 min, 40 cycles at 95 °C for 15 s, 60 °C for 34 s, and finally, 60 °C–95 °C with a heating rate of 0.3 °C/s. The expression of the target genes was normalized to that of *18S* or *GAPDH*. Relative gene expression was calculated using the $2^{-\Delta CT}$ formula.

Western blotting

Cells were lysed with radioimmunoprecipitation assay (RIPA) buffer with protease and phosphatase inhibitors phenylmethylsulfonyl fluoride (PMSF), sodium orthovanadate and sodium fluoride (all, Thermo Fisher Scientific, Germany) for measurement of protein concentration by BCA protein assay (Pierce Biotechnology Inc., U.S.). After blocking nonspecific binding with 5% (w/v) non-fat dry milk in TBS/T solution (DAKO, Denmark), the PVDF membrane (Millipore, Billerica, U.S.) was then incubated overnight at 4 °C with the primary antibodies anti-phospho-Smad3 (Cell Signaling Technology, U.S.), anti-Smad7 (Santa Cruz Biotechnology Inc., U.S.), and anti-glyceraldehyde-3-phosphate dehydrogenase (GAPDH; Santa Cruz Biotechnology Inc., U.S.), followed by a horseradish peroxidase-conjugated secondary antibody. Immunoreactive bands were detected by ECL reagents (Pierce Biotechnology Inc., U.S.).

Digital radiographs

The femurs of 6, 12 and 24 week old WT and KO mice were removed free of connective tissues, and subjected to Faxitron MX-20 Digital machine (Faxitron X-Ray Corp., Wheeling, IL, U.S.) under an exposure time of 6000 ms and a voltage of 32 kV.

Micro-computed tomography (μCT)

The metaphysis region of the left distal femurs of both groups at each time point was scanned using a μCT system (μCT40, Scanco Medical, Basserdorf, Switzerland), at custom isotropic resolution of 8-μm isometric voxel size with a voltage of 70 kV p and a current of 114 μA. Three-dimensional (3-D) reconstructions of mineralized tissues were performed by an application of a global threshold (211 mg hydroxyapatite/cm^3), and a Gaussian filter (sigma = 0.8, support = 2) was used to suppress noise. The scan range covered 3.2 mm above and 3.2 mm below the growth plate–epiphyseal junction, in total around 800 consecutive sections. From this region, a series of 100 slices between 80 μm and 880 μm distal to the growth plate–epiphyseal junction was chosen for the analysis. The regions of interest (ROIs) inside the bone tunnel, representing the trabecular bone, were separated with semi-automatically drawn contours (outer value of 512 and inner value of 33). After 3D reconstruction, the morphometric parameters including bone volume fraction (BV/TV),

Table 1
Primer sequences for quantitative real-time-polymerase chain reaction.

Gene name	Forward primer sequence	Reverse primer sequence	Product size (bp)
Runx2	GCCGGGAATGATGAGAACTA	GGACCGTCCACTGTCACTTT	200
Col1A1	GGCTCCTGCTCCTCTTAG	ACAGTCCAGTTCTTCATTGC	194
OCN	ATGGCTTGAAGACCGCCTAC	AGGGCAGAGAGAGAGGACAG	135
Adipsin	CCTGAACCCTACAAGCGATG	GGTTCCACTTCTTTGTCCTCG	170
C/EBPα	TTACAACAGGCCAGGTTTCC	CTCTGGGATGGATCGATTGT	232
TRAP	TCCTGGCTCAAAAAGCAGTT	ACATAGCCCACACCGTTCTC	212
CTR	CGGACTTTGACACAGCAGAA	CAGCAATCGACAAGGAGTGA	186
GAPDH	GCATGGCCTTCCGTGTTC	GATGTCATCATACTTGGCAGGTTT	86
18S rRNA	ACCATAAACGATGCCGACT	TGTCAATCCTGTCCGTGTC	216

bone mineral density (BMD, mg/cm^3), trabecular number (TbN, mm^{-1}), trabecular thickness (TbTh, mm), and trabecular separation (TbSp, mm), were calculated using built-in software [38].

Histology

The femurs were fixed in buffered formalin, embedded in paraffin, cut longitudinally into 5-μm thick sections and mounted on 3-aminopropyl-triethoxy-silane (Sigma-Aldrich, U.S.) coated slides. After deparaffination, the sections were stained with hematoxylin and eosin (H&E) staining, safranin-O (SO)/fast green staining, and examined under a light microscope (LEICA DMRB, Leica Cambridge Ltd., U.K.).

Bone histomorphometry

Both KO and WT mice at 24 weeks old were subcutaneously injected with double-fluorescence labelling (calcein green, 10 mg/kg & xylenol orange, 90 mg/kg) 13 days and 3 days respectively before sample collection. Samples of femur and tibia were dehydrated in graded concentrations of ethanol and embedded in methyl methacrylate (MMA). Sagittal sections for the left proximal femur were obtained at a thickness of 5 μm for Goldner Trichrome staining to analyze the static parameters, or at a thickness of 10 μm and left unstained for collection of fluorochrome-based data. A digitizing image analysis system (Osteometrics, Inc., USA) was used for quantitative bone histomorphometric measurements. Briefly, the regions of interest were the proximal femoral growth plate and the proximal femoral metaphysis located between 0.5 and 3 mm distal to the growth plate–epiphyseal junction. Parameters of osteoblast surface (Ob.S/BS, %; Ob.N/BS, mm^{-1}), osteoclast surface (Oc.S/BS, %; Oc.N/BS, mm^{-1}) and bone dynamic histomorphometric analyses for mineral apposition rate (MAR, μm/d) and bone formation rate per unit of bone surface (BFR/BS, μm/d ∗ 100) were recorded and compared. Images were obtained under a fluorescence microscope (Q500MC image analysis system, Leica, Germany), and light microscope (LEICA DMRB, Leica Cambridge Ltd., U.K.).

Data analysis

Data analysis was done using SPSS (version 16.0, SPSS Inc., U.S.). Comparisons of the gene expression among groups were performed using the ANOVA test, others were performed using the Mann–Whitney *U* test. Data was presented as mean ± SD. $p \leq 0.05$ was considered to be statistically significant.

Results

Femur morphometry at different time points

No significant difference of the size and length of the femurs between KO and WT groups at 6, 12, and 24 weeks old was observed by Digital radiographs (Fig. 1A). H&E staining and SO/fast green staining of the paraffin sections of femurs at 24 weeks old showed less trabecular bone around the metaphysic region and thinner growth plate in the

KO mice (Fig. 1B); 3-D reconstructed images of μCT also confirmed lower bone mass in the KO mice (Fig. 1B). The quantitative analysis of μCT data showed that the KO group had significantly decreased TbN ($p < 0.001$) and TbTh ($p = 0.010$), and increased TbSp ($p = 0.002$) in the metaphysic region of the femurs at 6 weeks old. At 12 weeks old, the KO group showed significantly decreased TbN ($p = 0.003$) and increased TbSp ($p = 0.009$) at this region. At 24 weeks old, the KO group had significantly decreased BMD ($p = 0.011$), BV/TV ($p = 0.010$), TbN ($p = 0.038$), and TbTh ($p = 0.018$), and increased TbSp ($p = 0.061$) (all n = 12; Fig. 1C). Figures from histology and parameters from μCT showed the decreased bone mass of the KO mice compared to WT with the age growth.

Bone histomorphometry analysis

Representative fluorescence micrographs of double labelling in trabecular surface (Tb.dL.S) showed a reduced interlabel width in the KO group (Fig. 2A). The statistical analysis of MAR confirmed a smaller mineral apposition rate in the KO group (Fig. 2D). The histomorphometric analysis atlas of overall distribution of distal femur showed a smaller amount of trabecular bone in the KO group (Fig. 2B). While the single labelled and double labelled length quantified by the BFR/BS did not show much difference between the two groups (Fig. 2E). Representative micrographs of MMA sections with Goldner Trichrome staining showed more osteoclasts in the KO group (Fig. 2C). The statistical analysis of Oc.S/BS and Oc.N/BS also confirmed a significant increase in the KO group, whereas the Ob.S/BS and Ob.N/BS did not show much difference (Fig. 2F) (all, n = 3).

Expression of mesenchymal stem cell-related surface markers

In order to compare the differentiation potential in vitro, BM-MSCs were obtained from both WT and KO femurs. MSC-related surface markers' expression in the BM-MSCs was measured using two positive isotype controls phycoerythrin (PE) and one negative isotype control fluorescein (FITC). The results of the cell surface markers' expression of BM-MSCs in the KO group were: CD90 (72.7%), CD44 (84.8%), Sca1 (97.1%), as well as CD34 (1.0%) and CD45 (0.4%) (Supplemental Fig. 1A). Similar results were found in the WT group: CD90 (70.5%), CD44 (81.8%) and Sca1 (91.6%), as well as CD34 (1.3%) and CD45 (0.8%) (Supplemental Fig. 1b).

Osteogenic potential of BM-MSCs in vitro

Under osteogenic inductive conditions, the BM-MSCs in the KO group had fewer mineralized nodules compared with those of the WT group both at day 7 and day 14 using Alizarin Red S staining confirmed by the quantification with acetic acid extraction method (Fig. 3A). The CFU-F assay and the quantification showed no significant difference between the colony forming efficiency of the two groups (Fig. 3B). Although cell proliferation reduced after osteogenic induction, there was no difference between the KO and WT groups (Fig. 3C). The ALP cytochemical staining showed lower ALP positive signal in the KO group
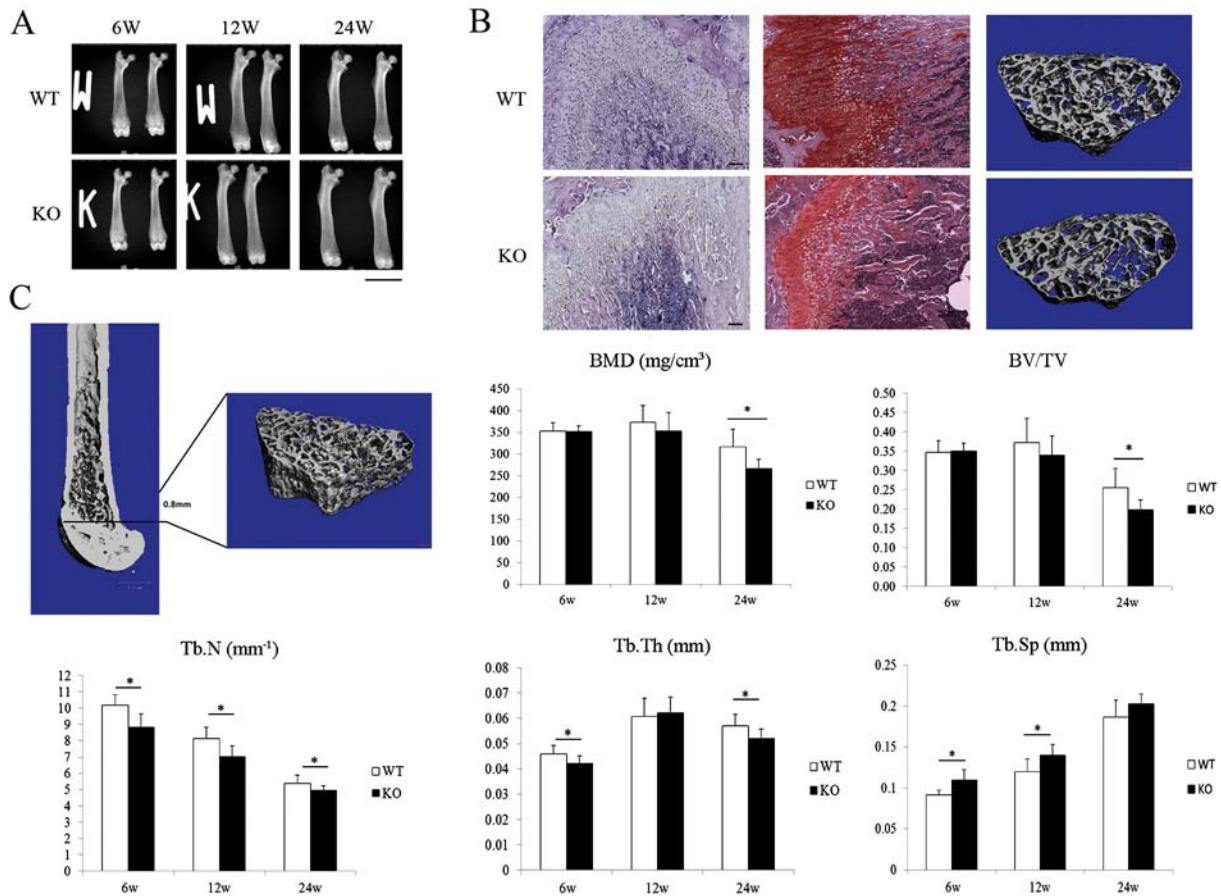
Fig. 1. (A) Representative digital X-ray images of the femurs of both KO and WT groups at 6, 12, and 24 weeks old. Scale bar = 6.5 mm. (B) Photomicrographs showing the trabecular bone around metaphysic region using H&E and SO/fast green staining of paraffin sections, as well as 3-D images of μCT showing the ROIs of the femurs from the 24 week old mice. Scale bar = 100 μm. (C) Column charts show the parameters of BMD, BV/TV, TbN, TbTh, TbSp of both KO and WT groups at 6, 12, and 24 weeks of age (all, n = 12). All data were shown as mean ± SD. *$p \leq 0.05$.

(Fig. 3D), and the ALP activity assay of the protein confirmed the results (Fig. 3E) (all above, n = 3). The gene expression of *Col1A1*, *Runx2* and *OCN* normalized to *GAPDH* was significantly lower in the KO group at day 7 and day 14 respectively compared with that of the WT group (n = 6; Fig. 3F). The expression of phospho-Smad3 in both the WT and KO groups with or without induction by osteogenic medium was compared. The expression was elevated in the KO group compared with the WT group under the osteogenic induction (Fig. 3G).

Adipogenic potential both in vivo and in vitro

The adipogenic potential induced by adipogenic medium of the BM-MSCs in the KO group had earlier lipid droplet formation at day 5 compared with the WT group (Fig. 4A). The Oil Red O staining showed more oil droplets in the KO group at day 21 (n = 3; Fig. 4B). The gene expression of *Adipsin* and *C/EBPα* normalized to *GAPDH* was significantly higher at day 7, day 14 and day 21 respectively in the KO group compared with that of the WT group (n = 6; Fig. 4C). The body weights at three time points were recorded and compared. Significantly higher weights were observed in the 12 and 24 week old groups of the KO animals (n = 12; Fig. 4D). The anatomy pictures also showed more fat tissue at the abdomen in the KO mice (Fig. 4E). H&E staining of the paraffin sections and Goldner Trichrome of the MMA sections in the metaphysic region of femurs at 24 weeks old showed more adipose tissue in the subchondral bone and bone marrow respectively in the KO animals (Figs. 4F & G).

Osteoclastogenic potential of BMMs in vitro

Osteoclasts were induced with M-CSF and RANKL in both groups, and more typical osteoclasts formed 3 days after induction in the KO group (Fig. 5A). The osteoclastogenic potential detected by TRAP staining was significantly higher in the KO group compared with that of the WT group (Fig. 5B). For quantification, TRAP positive cells with more than three nuclei were counted in each well of the 12-well plate selected and counted randomly for five visual fields (~4.9 mm²/field). The number and size of the osteoclasts were also higher and larger in the KO group than those of the WT group (Fig. 5E). The bone resorption assay and the quantification showed that the KO group had significantly larger resorptive areas (Figs. 5C & D) (all above, n = 3). The gene expression of *TRAP* and *CTR* normalized to *18S* was significantly higher in the KO group at day 7 compared with those of the WT group (n = 6; Fig. 5F). The expressions of phospho-Smad3 of both the WT and KO groups with or without induction by RANKL were compared. The expression was elevated in the KO group compared with the WT group by the RANKL-induced osteoclastogenesis (Fig. 5G).

Discussion

The importance of TGF-β in bone development and homeostasis has been extensively illustrated both in vitro and in vivo with convincing evidences showing the potent effects on bone formation, bone resorption, and the synergistic interplay between these two processes. This
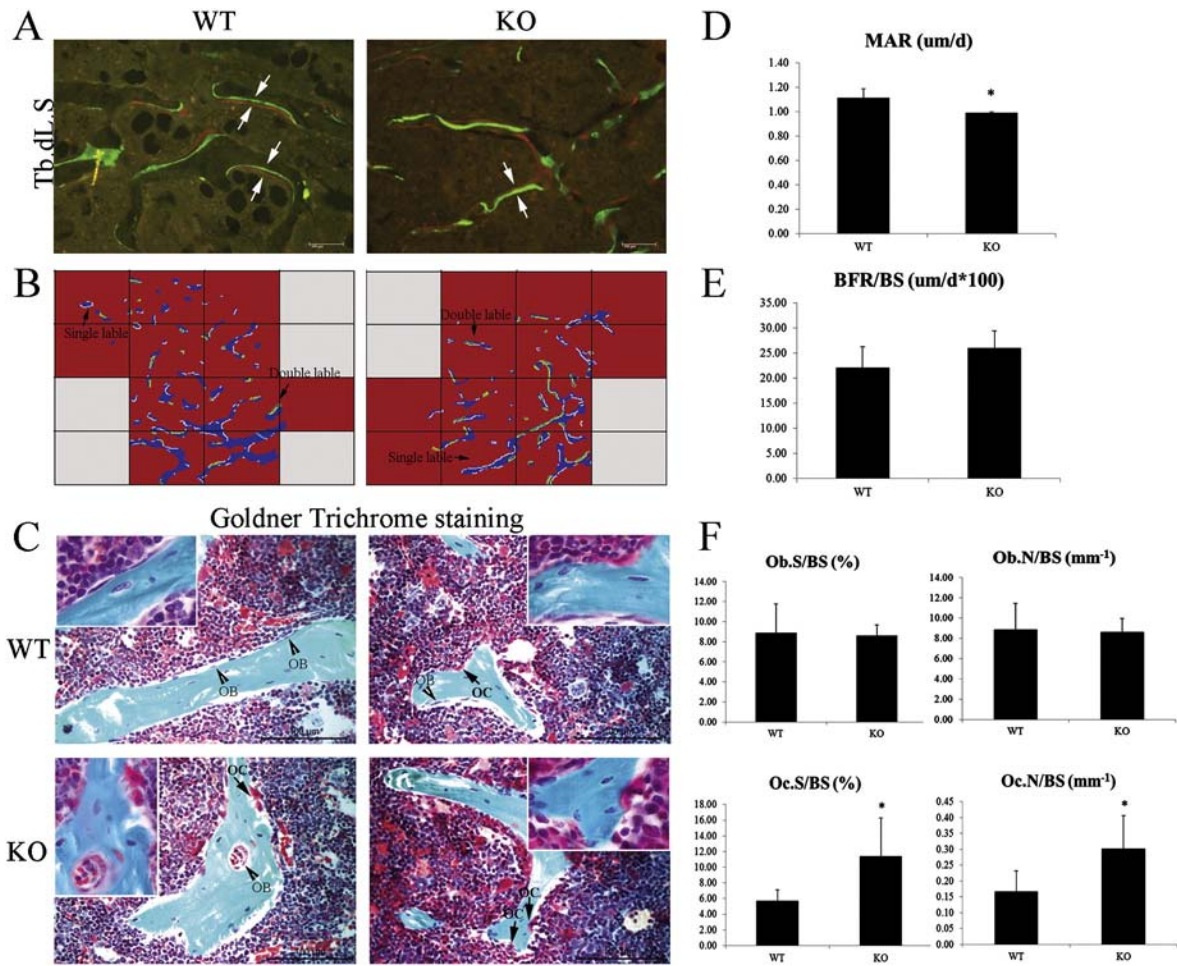
Fig. 2. (A) Representative fluorescence micrographs showing double labelling in trabecular surface (Tb.dL.S) in both WT and KO mice at 24 weeks old (arrows pointing to inter-labelling distances with double labelling by calcein green and xylenol orange). (B) Histomorphometry analysis atlas of overall distribution of trabecular bone, showing single labelling (white), double labelling (green & yellow) and trabecular bone (blue). (C) Representative photomicrographs for Goldner Trichrome staining of MMA sections in metaphysic region of femurs, showing both osteoblasts and osteoclasts (pointing by arrows). Photomicrographs with higher magnification ($\times 400$) were attached in the top corners. Scale bar = 100 μm. (D & E) Column charts showing statistics of MAR and BFR/BS. (F) Column charts showing parameters of osteoblast surface (Ob.S/BS, Ob.N/BS) and osteoclasts surface (Oc.S/BS and Oc.N/BS) (all, n = 3). All data were shown as mean ± SD. *$p < 0.05$.

universal cell regulator molecule plays an important role in holding the balance between the two tightly regulated processes [39]. Smad7, known as the inducible regulator, attunes the activities of TGF-β/Smad signaling pathway, and inhibits diverse cellular processes regulated by TGF-β, such as cell proliferation, differentiation, apoptosis, adhesion and migration. It is also involved in a vast majority of physiological events, and selected pathological processes including cancer, tissue fibrosis, diabetes, and some inflammatory diseases [23–29,40]. However, the essential role of Smad7 in bone remodeling during mammalian development has not yet been fully delineated. In our study, a transgenic animal with the deletion of Smad7 exon I is used to investigate the roles of Smad7 in bone remodeling. This Smad7 partial knockout animal has been widely adopted in the study of renal fibrosis for example. Previous studies showed that this kind of deletion is sufficient to generate experimental animals with higher TGF-β/Smad3 signaling activity [36]. Our study demonstrated that partial knockout of Smad7 impaired bone remodeling particularly in the process of bone resorption, as well as suppressing osteogenesis and promoting osteoclastogenesis, indicating Smad7 itself may be an important regulator in both processes.

We found that functional impairment of Smad7 on bone morphometry becomes more prominent in the increasingly older KO mice. The parameters of BMD and BV/TV only showed significant decreases at 24 weeks in the KO group, indicating the accumulated reduction on bone mass in the KO group. The significant changes shown in measured

trabecular bone microarchitecture are of clinical significance, since biomechanical strength is closely associated with fracture risk [41]. This interpretation has important clinical relevance and invites therapeutic possibilities with age. Another interesting observation is the decreased trabecular bone mass as shown in both μCT and bone histomorphometry analysis, which is mainly due to enhanced bone resorption (increased number and activity of osteoclasts). In perfectly balanced bone remodeling, bone formation and resorption are strictly coordinated. The activated osteoclasts are most necessary for the control of bone formation in the bone remodeling process [42,43]. It has been confirmed recently in another study, that osteoclastic bone resorption can directly activate osteoblast function, through regulating the cell signals in bone formation [44]. However, in our current study, we did not see any significant decrease in the number and activity of osteoblasts in vivo in the KO mice, indicating the compensatory work of the strongly upregulated bone resorption event, which may be the main contributor for the reduced bone mass.

Previous studies have demonstrated that TGF-β plays a vital role in every stage of osteogenesis in vitro. However, some ambiguous observations with conflicting interpretations may be attributed to the different differentiation stages of the target cell populations. One important variable is that TGF-β can stimulate the early stages of differentiation but inhibit in later stages [45,46]. These studies support our findings that the canonical TGF-β signaling (as shown by the expression of
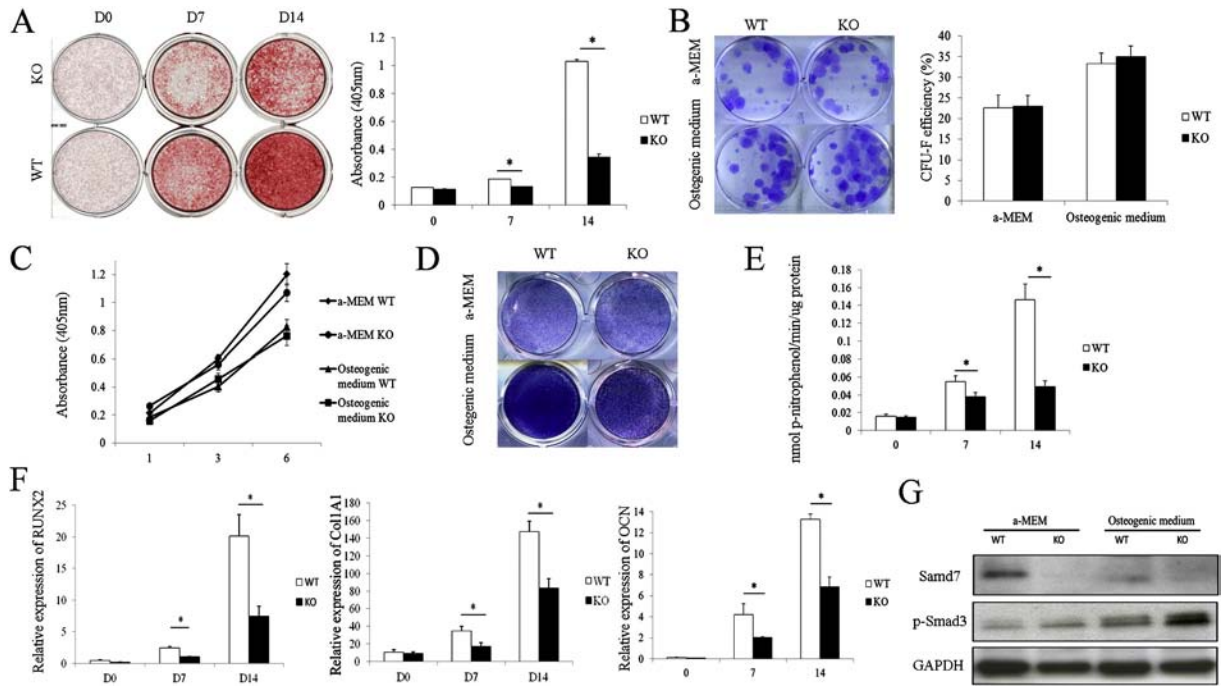
Fig. 3. (A) Photomicrographs and column chart showing Alizarin Red S staining and quantification at days 0, 7, and 14 in both KO and WTBM-MSCs under osteogenic culture conditions. (B) Photomicrographs and column chart showing the CFU-F efficiency at day 10. (C) Column chart showing the cell proliferation quantification using BrdU assay at days 1, 3, and 6. (D) Photomicrographs showing the ALP cytochemical staining at day 14. (E) Column chart showing the ALP activity at day 14 (n = 3, all the above). (F) Column charts showing the relative gene expression of *Runx2*, *Col1A1* and *OCN* normalized to *GAPDH* at days 0, 7, and 14 (n = 6). (G) Electrophoresis images showing Smad7 and phospho-Smad3 expression patterns. All data were shown as mean ± SD. *$p \leq 0.05$.

phospho-Smad3) was enhanced and triggered early osteogenesis in both WT and KO groups; while overstimulated canonical TGF-β signaling in the later process of osteogenesis resulted in reduced osteoblastogenic potential. The decrease in TβRI and TβRII expression was observed during human BM-MSC osteogenic differentiation from osteoprogenitor cells to mature osteoblasts [47], and TGF-β/receptor interactions were reduced during murine and rat osteoblast differentiation [48,49]. Smad3, activated by TGF-β1, physically interacts with
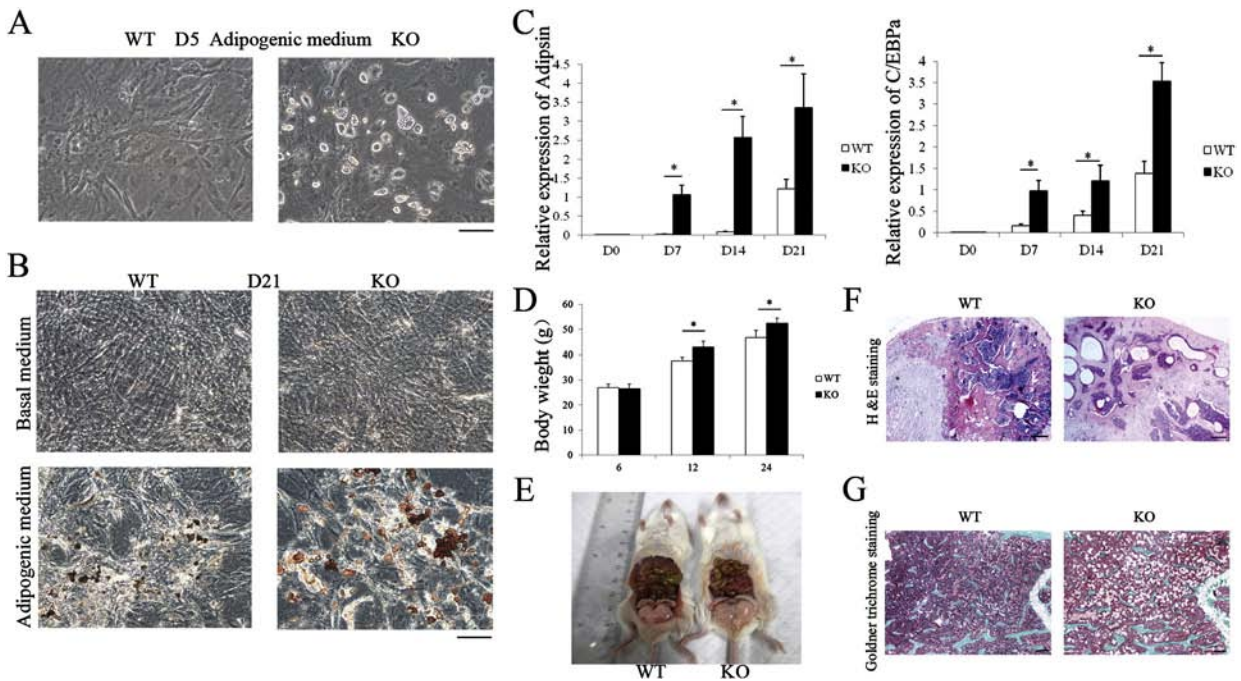

Fig. 4. (A) Photomicrographs showing the lipid droplet formation after adipogenic induction at day 5 of BM-MSCs. (B) Photomicrographs showing Oil Red O staining of BM-MSCs in both groups cultured with basal medium or adipogenic medium at day 21 (n = 3). Scale bar = 100 μm. (C & D) Column charts showing the relative gene expression of *Adipsin* and *C/EBPα* normalized to *GAPDH* at days 0, 7, 14, and 21 (n = 6). (D) Column charts showing the body weight of mice at 6, 12 and 24 weeks old (n = 12). (E) Photo showing the fat tissue exposed in abdomen in both KO and WT mice. (F) Photomicrographs showing adipose tissues in the subchondral bone and bone marrow of the KO animals by H&E staining on paraffin sections and Goldner Trichrome staining on MMA sections at the age of 24 weeks old compared with WT. Scale bar = 200 μm. All data were shown as mean ± SD. *$p \leq 0.05$.
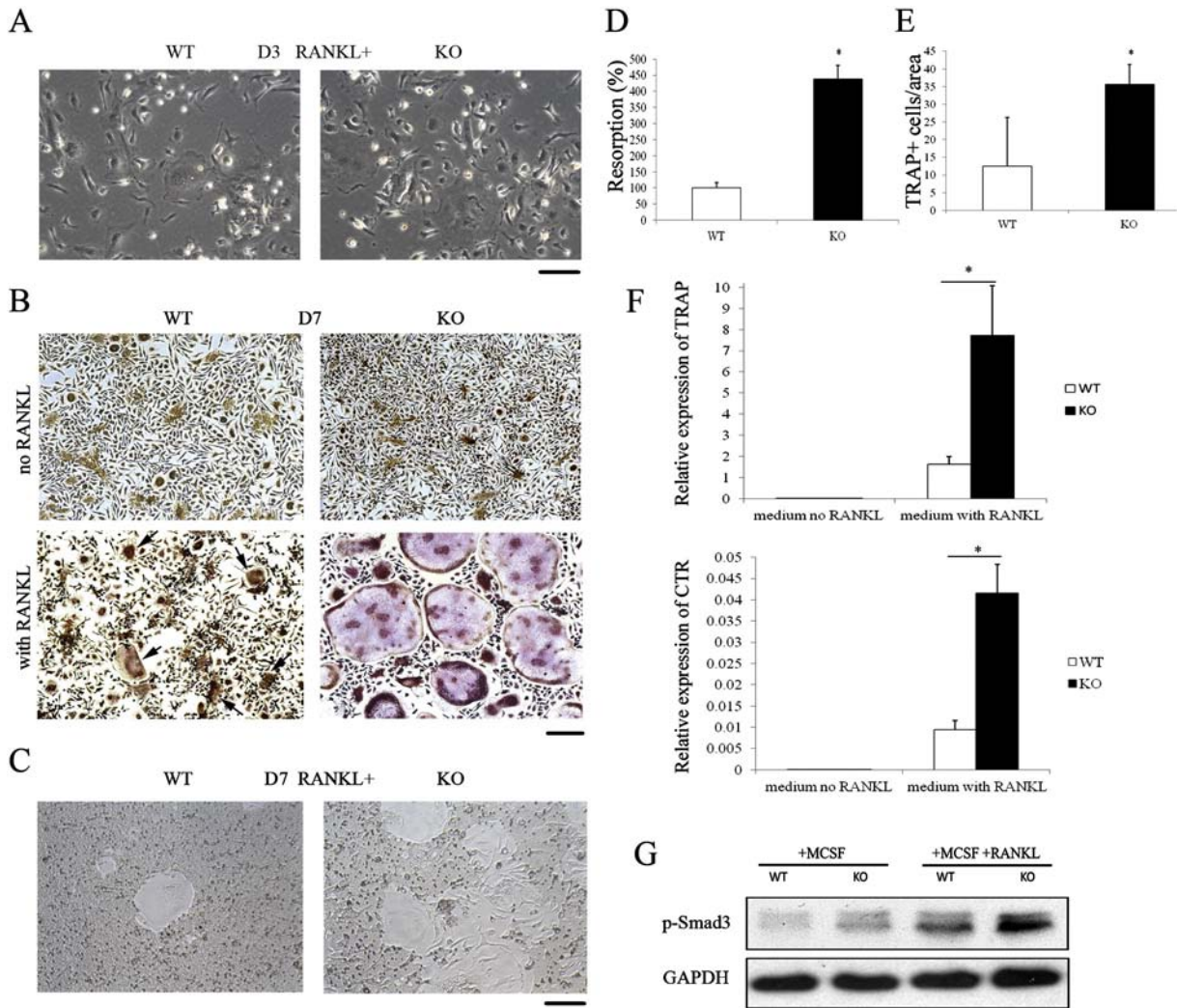
Fig. 5. (A) Photomicrographs showing the osteoclast-likecell formation after RANKL induction at day 3 in both KO and WT groups. (B) Photomicrographs showing BMMs of both KO and WT groups cultured with or without RANKL and stained with TRAP (arrows showing the osteoclasts in WT group). (C) Photomicrographs showing the bone resorption activity of the osteoclasts using OSSA plate. (D) Column charts showing the bone resorption area per well measured by an image analyzer. (E) Column charts showing statistics of TRAP + osteoclast number counted in five visual areas at random per well of the 12-well plates (n = 3, all the above). (F) Column charts showing the relative gene expression of *TRAP* and *CTR* normalized to *18S* at day 7 (n = 6). (G) Electrophoresis images showing phospho-Smad3 expression. All scale bar = 200 μm. All data were shown as mean ± SD. *$p \leq 0.05$.

Runx2 at the Runx2-responsive elements, thus suppressing the expression of Runx2 and other osteogenic markers like *Col1A1*, *ALP*, and *osteocalcin* by an autoregulatory feedback mechanism to slow down bone formation [45]. Moreover, menin, a repressor of osteoblast maturation by binding to TGF-β1-activated Smad3, mediates the inhibitory effects of the latter on Runx2 activity [50]. Given all these results and observations, it is expected that loss of Smad7 would suppress osteogenic potential, which is in agreement with our findings: partial loss of Smad7 function may inhibit the osteogenesis process through activating TGF-β/Smad3 signaling.

TGF-β is released in active form during bone resorption, and increases RANKL/OPG ratio in vitro, which can enhance osteoclastogenesis [51–54]. The direct effects of TGF-β1 on osteoclast precursors, such as up-regulation of RANK expression [32,52], induction of NF-κB activation [33], and suppression of cytokine signaling expression [34], are responsible for the promotion of TGF-β1 on osteoclastogenesis. TGF-β stimulates RANKL-induced osteoclastogenesis through molecular interaction with Smad3 and Traf6 [55]. In the current study, we demonstrated an important involvement of Smad7 in osteoclastogenesis, through activating the expression of phospho-Smad3. Given that Smad7 is the crosstalk mediator for both canonical and non-canonical TGF-β signaling networks, and the intricate regulation between these two pathways

[10], the exact mechanisms by which Smad7 regulates osteogenesis and osteoclastogenesis need further and deeper investigation.

Our study demonstrated the possible involvement of Smad7 in bone remodeling, via regulating osteogenesis and osteoclastogenesis. Although a number of questions still remain unanswered, the manipulation of Smad7 may represent a new strategy for the treatment of metabolic bone diseases such as osteoporosis. The role of Smad7 in osteoporotic bone remodeling, bone fracture healing and possible pharmacological intervention in Smad-based pathways deserve further studies. In addition, the KO mice also exhibited impaired capacity to balance between osteogenesis and adipogenesis based on our observation. After all, it is known that C/EBPα regulates the balance between osteogenesis and adipogenesis through modulation of DNA methylation and histone acetylation [56]. So how the Smad7 regulates the switch between osteogenesis and adipogenesis remains unclear. Furthermore, the thinner growth plate of KO mice femurs observed in our study, and the proven role of Smad7 in chondrocyte differentiation [31], and tissue fibrosis [28,57], do suggest a regulatory role of Smad7 in chondrogenesis and fibrosis as well.

In summary, our current study demonstrates that partial loss of Smad7 function in a living mouse model leads to impaired bone remodeling particularly in the process of bone resorption process in vivo, as

well as suppressed osteogenesis and enhanced osteoclastogenesis in vitro. These findings may provide new evidence for a better understanding of the biological functions of Smad7 in bone remodeling, and a novel Smad-based therapeutic potential for metabolic bone diseases. Smad7 itself may be a potential new target for maintaining bone health.

Conclusion

The trabecular number, trabecular thickness and MAR were significantly decreased in the Smad7$^{\Delta E1}$ mice, indicating a trend towards bone loss, which was supported by measurements of increased trabecular separation and osteoclast surface compared with the WT mice. The Smad7$^{\Delta E1}$ mice had impaired bone remodeling associated with enhanced bone resorption. Partial loss of Smad7 inhibited osteogenesis and promoted adipogenesis in BM-MSCs as well as osteoclastogenesis in BMMs. Altogether the results indicate that Smad7 is involved in regulating bone remodeling and the maintenance of bone homeostasis. Any disruption to Smad7 expression or activity could therefore play prominent roles in various metabolic bone diseases. Smad7 may be a new ideal therapeutic target for maintaining or restoring proper bone health.

Supplementary data to this article can be found online at http://dx.doi.org/10.1016/j.bone.2014.06.033.

References

[1] Li Z, Kong K, Qi W. Osteoclast and its roles in calcium metabolism and bone development and remodeling. Biochem Biophys Res Commun 2006;343:345–50.
[2] Hill P. Bone remodeling. Br J Orthod 1998;25:101–7.
[3] Sumner DR, Turner TM, Cohen M, Losavio P, Urban RM, Nichols EH, et al. Aging does not lessen the effectiveness of TGFbeta2-enhanced bone regeneration. J Bone Miner Res 2003;18:730–6.
[4] Feng XH, Derynck R. Specificity and versatility in TGF-β signaling through Smads. Annu Rev Cell Dev Biol 2005;21:659–93.
[5] Shi Y, Massague J. Mechanisms of TGF-β signaling from cell membrane to the nucleus. Cell 2003;113:685–700.
[6] Nakao A, Okumura K, Ogawa H. Smad7: a new key player in TGF-β-associated disease. Trends Mol Med 2002;8:361–3.
[7] Park SH. Fine tuning and cross-talking of TGF-β signal by inhibitory Smads. J Biochem Mol Biol 2005;38:9–16.
[8] Yan X, Liu Z, Chen Y. Regulation of TGF-β signaling by Smad7. Acta Biochim Biophys Sin 2009;41:263–72.
[9] Lonn P, Moren A, Raja E, Dahl M, Moustakas A. Regulating the stability of TGF-β receptors and Smads. Cell Res 2009;19:21–35.
[10] Yan X, Chen YG. Smad7: not only a regulator, but also a cross-talk mediator of TGF-β signaling. Biochem J 2011;434:1–10.
[11] Nakao A, Afrakhte M, Moren A, Nakayama T, Christian JL, Heuchel R, et al. Identification of Smad7, a TGF-β-inducible antagonist of TGF-β signalling. Nature 1997;389:631–5.
[12] Hayashi H, Abdollah S, Qiu Y, Cai J, Xu YY, Grinnell BW, et al. The MAD-related protein Smad7 associates with the TGFβ receptor and functions as an antagonist of TGFβ signaling. Cell 1997;89:1165–73.
[13] Souchelnytskyi S, Nakayama T, Nakao A, Moren A, Heldin CH, Christian JL, et al. Physical and functional interaction of murine and *Xenopus* Smad7 with bone morphogenetic protein receptors and transforming growth factor-β receptors. J Biol Chem 1998;273:25364–70.
[14] Kavsak P, Rasmussen RK, Causing CG, Bonni S, Zhu H, Thomsen GH, et al. Smad7 binds to Smurf2 to form an E3 ubiquitin ligase that targets the TGF β receptor for degradation. Mol Cell 2000;6:1365–75.
[15] Ebisawa T, Fukuchi M, Murakami G, Chiba T, Tanaka K, Imamura T, et al. Smurf1 interacts with transforming growth factor-beta type I receptor through Smad7 and induces receptor degradation. J Biol Chem 2001;276:12477–80.
[16] Suzuki C, Murakami G, Fukuchi M, Shimanuki T, Shikauchi Y, Imamura T, et al. Smurf1 regulates the inhibitory activity of Smad7 by targeting Smad7 to the plasma membrane. J Biol Chem 2002;277:39919–25.
[17] Gronroos E, Hellman U, Heldin CH, Ericsson J. Control of Smad7 stability by competition between acetylation and ubiquitination. Mol Cell 2002;10:483–93.
[18] Yan X, Lin Z, Chen F, Zhao X, Chen H, Ning Y, et al. Human BAMBI cooperates with Smad7 to inhibit transforming growth factor-β signaling. J Biol Chem 2009;284:30097–104.
[19] Simonsson M, Heldin CH, Ericsson J, Gronroos E. The balance between acetylation and deacetylation controls Smad7 stability. J Biol Chem 2005;280:21797–803.
[20] Kume S, Haneda M, Kanasaki K, Sugimoto T, Araki S, Isshiki K, et al. SIRT1 inhibits transforming growth factor β-induced apoptosis in glomerular mesangial cells via Smad7 deacetylation. J Biol Chem 2007;282:151–8.
[21] Ulloa L, Doody J, Massague J. Inhibition of transforming growth factor-β/SMAD signalling by the interferon-γ/STAT pathway. Nature 1999;397:710–3.
[22] Bitzer M, von Gersdorff G, Liang D, Dominguez-Rosales A, Beg AA, Rojkind M, et al. A mechanism of suppression of TGF-β/SMAD signaling by NF-κB/RelA. Genes Dev 2000;14:187–97.
[23] Fidler IJ. Blockade of the TGF-β superfamily by Smad7: breaking a link in the metastatic chain. J Natl Cancer Inst 2005;97:1714–5.
[24] Liu X, Lee J, Cooley M, Bhogte E, Hartley S, Glick A. Smad7 but not Smad6 cooperates with oncogenic ras to cause malignant conversion in a mouse model for squamous cell carcinoma. Cancer Res 2003;63:7760–8.
[25] Halder SK, Rachakonda G, Deane NG, Datta PK. Smad7 induces hepatic metastasis in colorectal cancer. Br J Cancer 2008;99:957–65.
[26] Kleeff J, Ishiwata T, Maruyama H, Friess H, Truong P, Buchler MW, et al. The TGF-β signaling inhibitor Smad7 enhances tumorigenicity in pancreatic cancer. Oncogene 1999;18:5363–72.
[27] Broderick P, Carvajal-Carmona L, Pittman AM, Webb E, Howarth K, Rowan A, et al. A genome-wide association study shows that common alleles of SMAD7 influence colorectal cancer risk. Nat Genet 2007;39:1315–7.
[28] Wang B, Hao J, Jones SC, Yee MS, Roth JC, Dixon IM. Decreased Smad7 expression contributes to cardiac fibrosis in the infarcted rat heart. Am J Physiol Heart Circ Physiol 2002;282:1685–96.
[29] Lan HY. Transforming growth factor-β/Smad signaling in diabetic nephropathy. Clin Exp Pharmacol Physiol 2012;39:731–8.
[30] Kawakatsu M, Kanno S, Gui T, Gai Z, Itoh S, Tanishima H, et al. Loss of Smad3 gives rise to poor soft callus formation and accelerates early fracture healing. Exp Mol Pathol 2011;90:107–15.
[31] Iwai T, Murai J, Yoshikawa H, Tsumaki N. Smad7 inhibits chondrocyte differentiation at multiple steps during endochondral bone formation and down-regulates p38 MAPK pathways. J Biol Chem 2008;283:27154–64.
[32] Yan T, Riggs BL, Boyle WJ, Khosla S. Regulation of osteoclastogenesis and RANK expression by TGF-1. J Cell Biochem 2001;83:320–5.
[33] Kaneda T, Nojima T, Nakagawa M, Ogasawara A, Kaneko H, Sato T, et al. Endogenous production of TGF-beta is essential for osteoclastogenesis induced by a combination of receptor activator of NF-kappa B ligand and macrophage-colony-stimulating factor. J Immunol 2000;165:4254–63.
[34] Fox SW, Haque SJ, Lovibond AC, Chambers TJ. The possible role of TGF-β-induced suppressors of cytokine signaling expression in osteoclast/macrophage lineage commitment in vitro. J Immunol 2003;170:3679–87.
[35] Li R, Rosendahl A, Brodin G, Cheng AM, Ahgren A, Sundquist C, et al. Deletion of exon I of SMAD7 in mice results in altered B cell responses. J Immunol 2006;176:6777–84.
[36] Chen HY, Huang XR, Wang W, Li JH, Heuchel RL, Chung AC, et al. The protective role of Smad7 in diabetic kidney disease: mechanism and therapeutic potential. Diabetes 2011;60:590–601.
[37] Gregory CA, Gunn WG, Peister A, Prockop DJ. An Alizarin red-based assay of mineralization by adherent cells in culture: comparison with cetylpyridinium chloride extraction. Anal Biochem 2004;329:77–84.
[38] Peng S, Zhang G, He YX, Wang X, Leung P, Leuang K, et al. Epimedium-derived falvonoids promote osteoblastogenesis and suppress adipogenesis in bone marrow stromal cells while exerting an anabolic effect on osteoporotic bone. Bone 2009;45:534–44.

[39] Mundy GR. The effects of TGF-beta on bone. Ciba Found Symp 1991;157:137–43 [discussion 143–151].

[40] Xin X, Li XH, Wu JZ, Chen KH, Liu Y, Nie CJ, et al. Pentamethylquercetin ameliorates fibrosis in diabetic Goto-Kakizaki rat kidneys and mesangial cells with suppression of TGF-β/Smads signaling. Eur J Pharmacol 2013;713:6–15.

[41] Boutroy S, Van Rietbergen B, Sornay-Rendu E, Munoz F, Bouxsein ML, Delmas PD. Finite element analysis based on in vivo HR-pQCT images of the distal radius is associated with wrist fracture in postmenopausal women. J Bone Miner Res 2008;23:392–9.

[42] Sims NA, Martin TJ. Coupling the activities of bone formation and resorption: a multitude of signals within the basic multicellular unit. BoneKEy Reports 3 Article number: 481; 2014.

[43] Martin TJ, Sims NA. Osteoclast-derived activity in the coupling of bone formation to resorption. Trends Mol Med 2005;11:76–81.

[44] Udagawa Nobuyuki. Osteoclastic bone resorption directly activates osteoblast function. Arthritis Res Ther 2012;14(Suppl. 1):O26.

[45] Alliston T, Choy L, Ducy P, Karsenty G, Derynck R. TGF-beta-induced repression of CBFA1 by Smad3 decreases cbfa1 and osteocalcin expression and inhibits osteoblast differentiation. EMBO J 2001;20:2254–72.

[46] Maeda S, Hayashi M, Komiya S, Imamura T, Miyazono K. Endogenous TGF-β signaling suppresses maturation of osteoblastic mesenchymal cells. EMBO J 2004;23:525–63.

[47] Walsh S, Jefferiss C, Stewart K, Beresford JN. TGF 1 limits the expansion of the osteoprogenitor fraction in cultures of human bone marrow stromal cells. Cell Tissue Res 2003;311:187–98.

[48] Centrella M, Casinghino S, Kim J, Pham T, Rosen V, Wozney J, et al. Independent changes in type I and type II receptors for transforming growth factor beta induced by bone morphogenetic protein 2 parallel expression of the osteoblast phenotype. Mol Cell Biol 1995;15:3273–81.

[49] Takeuchi Y, Nakayama K, Matsumoto T. Differentiation and cell surface expression of transforming growth factor-beta receptors are regulated by interaction with matrix collagen in murine osteoblastic cells. J Biol Chem 1996;271:3938–44.

[50] Sowa H, Kaji H, Hendy GN, Canaff L, Komori T, Sugimoto T, et al. Menin is required for BMP-2-and TGF-β-regulated osteoblastic differentiation through interaction with Smads and Runx2. J Biol Chem 2004;279:40267–75.

[51] Sells Galvin RJ, Gatlin CL, Horn JW, Fuson TR. TGF-beta enhances osteoclast differentiation in hematopoietic cell cultures stimulated with RANKL and M-CSF. Biochem Biophys Res Commun 1999;265:233–9.

[52] Fuller K, Lean JM, Bayley KE, Wani MR, Chambers TJ. A role for TGF-beta1 in osteoclast differentiation and survival. J Cell Sci 2000;113:2445–53.

[53] Jurado S1, Garcia-Giralt N, Díez-Pérez A, Esbrit P, Yoskovitz G, Agueda L, et al. Effect of IL-1beta, PGE(2), and TGF-beta1 on the expression of OPG and RANKL in normal and osteoporotic primary human osteoblasts. J Cell Biochem 2010;110:304–10.

[54] Kasagi S, Chen W. TGF-beta1 on osteoimmunology and the bone component cells. Cell Biosci 2013;3:1–7.

[55] Yasui T, Kadono Y, Nakamura M, Oshima Y, Matsumoto T, Masuda H, et al. Regulation of RANKL-induced osteoclastogenesis by Smad3 through molecular interaction between Smad3 and Traf6. J Bone Miner Res 2011;26:1447–56.

[56] Zhao QH, Wang SG, Liu SX, Li JP, Zhang YX, Sun ZY, et al. PPARγ forms a bridge between DNA methylation and histone acetylation at the C/EBPα gene promoter to regulate the balance between osteogenesis and adipogenesis of bone marrow stromal cells. FEBS J 2013;280:5801–14.

[57] Liu GX, Li YQ, Huang XR, Wei L, Chen HY, Shi YJ, et al. Disruption of Smad7 promotes ANG II-mediated renal inflammation and fibrosis via Sp1-TGF-β/Smad3-NF.κB-dependent mechanisms in mice. PLoS One 2013;8:e53573.